A Novel Transform for Ultra-Wideband Multi-Static Imaging Radar

Takuya Sakamoto
Graduate School of Informatics
Kyoto University
Yoshida-Honmachi, Sakyo-ku, Kyoto 606-8501
Email: t-sakamo@i.kyoto-u.ac.jp

Toru Sato
Graduate School of Informatics
Kyoto University
Yoshida-Honmachi, Sakyo-ku, Kyoto 606-8501
Email: tsato@kuee.kyoto-u.ac.jp

***Abstract*—Ultra-wideband (UWB) radar is considered to be a promising candidate for next-generation imaging systems in a variety of fields. The UWB radar imaging method known as SEABED (Shape Estimation Algorithm Based on Extraction of Directly Scattered Waves) has been of particular interest because of its high-speed imaging capability. This method was designed to employ a mechanical scanner that required a long measuring time, preventing real-time operation. One solution for this problem is the introduction of antenna array systems. By using an antenna array, multi-static data are obtained but cannot be effectively processed with the SEABED method because it was designed for mono-static data. A high-speed imaging method, namely Bistatic SEABED, has been proposed for UWB multi-static radar data. This method employs a reversible transform called Bistatic inverse boundary scattering transform (IBST) derived for a fixed distance between transmitting and receiving antennas. This study derives another transform, namely the common midpoint IBST, for a fixed midpoint between transmitting and receiving antennas. The performance of these methods is investigated through numerical simulations**

I. Introduction

Development of an advanced sensor system can make it possible for robots to be deployed in emergency situations like cases of intense fire or nuclear plant accidents. For this purpose, an ultra-wideband (UWB) radar is promising because unlike conventional camera-based systems, it has excellent range-resolution and is able to obtain three-dimensional images. A number of methods have been proposed to obtain a target image using UWB radars [1], [2], [3]. One promising method among them is the Shape Estimation Algorithm Based on Extraction of Directly Scattered Waves (SEABED) method that uses the delay time of echoes and the reversible transform, namely the IBST (inverse boundary scattering transform) because of its real-time imaging realized by high-speed processing [4], [5].

The SEABED method [4] is designed for a mono-static radar system anduses a single antenna scanned along a straight line. This system is capable of obtaining images within a short period of time, while taking much longer to measure the data, which spoils the high-speed imaging processing. A radar system with an antenna array is a solution to this issue [6]. This system can realize high-speed measurement because it does not use mechanical scanning. The system selects the transmitting and receiving antenna electrically with a switch. This system also enables a multi-static radar system that uses two different antennas for transmitting and receiving. To make the measurement even faster, orthogonal modulation has been proposed [7] and this scheme has realized simultaneous transmission from multiple antennas.

These measurement schemes using array antennas enabel bistatic radar measurement that uses different antennas for transmitting and receiving. Since the original IBST cannot be applied to the bistatic measurement data, another transform called the Bistatic-IBST has been developed [6] and used for a radar system with an antenna array. The Bistatic-IBST assumes antenna scanning with a fixed distance between the transmitting and receiving antennas. Therefore, this method does not fully use all the information contained in the data and restricts its imaging performance. This paper derives another transform, the common mid-point (CMP)-IBST that assumes a fixed midpoint between the transmitting and receiving antennas. The imaging performance of the CMP-IBST is compared with other conventional transforms.

II. System Model

Let us assume a two-dimensional inverse scattering problem. We use a linear antenna array with fixed intervals between antennas, where the antennas are located on the x-axis. Figure 1 shows the antenna layout and assumed coordinate system. The system is a multi-static radar and each UWB antenna is connected to the transmitter and receiver via a switch. We define $(X_n, 0)$ as the position of the n-th antenna. The target is located in the half-space $y > 0$. $s(X_m, X_n; t)$ is a received signal using the m-th and n-th antennas for transmitting and receiving, respectively. A matched filter is applied to the received signals so that the peak of the echo signal exactly corresponds to the echo delay. Assuming an N-element antenna array, N^2 signals $s(X_m, X_n; t)$ $(m, n = 1, 2, \cdots, N)$ are received for multi-static measurement. Though the positions of transmitting and receiving antennas X_m and X_n are discrete numbers, they are treated as continuous numbers in the following sections for simplicity. For example, the received signals are expressed as $s(X_\mathrm{t}, X_\mathrm{r}; t)$, where X_t and X_r are the positions of the transmitting and receiving antennas.

978-1-4577-0919-7/12/$26.00 ©2011 IEEE

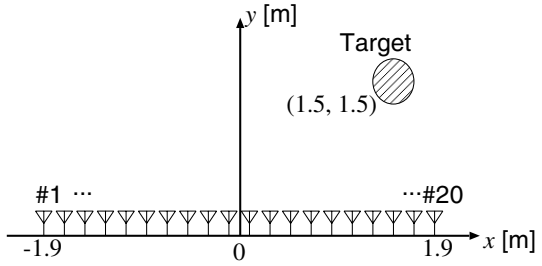

Fig. 1. System model.

A significant advantage of the SEABED method is that it uses only peak points of echoes instead of their entire waveforms, making the processing fast. Suppose the variable Y defined as $Y = ct_{\rm d}/2$ using a propagation speed c and one of the delay time values t that is estimated with a signal $s(X_{\rm t}, X_{\rm r}; t)$. Y is the distance between the antenna and scattering center for a mono-static radar. As Y depends on $(X_{\rm t}, X_{\rm r})$, we express this variable as a function $Y(X_{\rm t}, X_{\rm r})$. We assume that $Y(X_{\rm t}, X_{\rm r})$ has a single value, although in general there are multiple Y values for each transmitting/receiving antenna pair. This curved surface $Y(X_{\rm t}, X_{\rm r})$ is called a quasi-wavefront (QW). The problem we deal with in this paper is to estimate a target shape using the given data $Y(X_{\rm t}, X_{\rm r})$.

III. Conventional Bistatic-IBST

We now present the derivation of the conventional Bistatic-IBST [6]. A QW $Y(X_{\rm t}, X_{\rm r})$ is half the summation of the distance between the transmitting antenna and a scattering center (x, y) $\sqrt{(X_{\rm t} - x)^2 + y^2}$ and the distance between the receiving antenna and the scattering center $\sqrt{(X_{\rm r} - x)^2 + y^2}$. Therefore, the actual scattering center (x, y) must be on the ellipse with foci $(X_{\rm t}, 0)$ and $(X_{\rm r}, 0)$.

This ellipse can be expressed as the middle point of the m-th transmitting and the n-th receiving antennas $X_{\rm a} = (X_m + X_n)/2$ and half the difference between the transmitting and receiving antenna positions $X_{\rm s} = (X_m - X_n)/2$. Note that $X_{\rm s}$ can be a negative number. The ellipse is expressed as

$$\begin{aligned} G(x, y; X_{\rm a}, X_{\rm s}) &= Y^4 - \{{X_{\rm s}}^2 + y^2 + (X_{\rm a} - x)^2\}Y^2 \\ &\quad + {X_{\rm s}}^2 (X_{\rm a} - x)^2 = 0. \end{aligned} \tag{1}$$

The partial derivative of Eq. (1) in terms of $X_{\rm a}$ must be zero for the actual scattering center (x, y) as

$$\frac{\partial G(x, y; X_{\rm a}, X_{\rm s})}{\partial X_{\rm a}} = 0. \tag{2}$$

Solving these simultaneous equations (1) and (2) for x to obtain

$$x = X_{\rm a} - \frac{2Y^3 \frac{\partial Y}{\partial X_{\rm a}}}{Y^2 - {X_{\rm s}}^2 + \sqrt{\left(Y^2 - {X_{\rm s}}^2\right)^2 + 4{X_{\rm s}}^2 Y^2 \left(\frac{\partial Y}{\partial X_{\rm a}}\right)^2}}. \tag{3}$$

Solving Eq. (1) for y to obtain

$$y = \frac{\sqrt{Y^2 - {X_{\rm s}}^2}}{Y} \sqrt{Y^2 - (x - X_{\rm a})^2}, \tag{4}$$

where x has been already calculated with Eq. (3). Eqs. (3) and (4) are called Bistatic-IBST, which is used for fast imaging using a multi-static radar.

Substituting $X_{\rm s} = 0$ into Eq. (3), we obtain

$$x = X - Y \partial Y / \partial X_{\rm a}, \tag{5}$$

which is called the IBST that is used for the original SEABED method. In the case of IBST, the ellipse in Eq. (1) shrinks to a circle.

IV. Proposed Common-Midpoint IBST

We derive another transform that differs from the Bistatic-IBST described in the previous section. In the previous section, Eq. (1) was differentiated in terms of $X_{\rm a}$ to obtain the scattering center (x, y). In this section, we differentiate the equation in terms of $X_{\rm s}$ and this derivative should also be zero as

$$\frac{\partial G(x, y; X_{\rm a}, X_{\rm s})}{\partial X_{\rm s}} = 0. \tag{6}$$

By partially differentiating Eq. (1) in terms of$X_{\rm s}$ we obtain

$$\begin{aligned} \frac{\partial G}{\partial X_{\rm s}} &= 2\frac{\partial Y}{\partial X_{\rm s}} Y^3 - X_{\rm s} Y^2 - \left\{{X_{\rm s}}^2 + y^2 + (x - X)^2\right\} \\ &\quad \frac{\partial Y}{\partial X_{\rm s}} Y - (x - X)^2 {X_{\rm s}}^2. \end{aligned} \tag{7}$$

Substituting Eq. (7) into Eq. (6) and solving it for x, we obtain

$$x = X_{\rm a} - Y \sqrt{\frac{Y(X_{\rm s} - Y\frac{\partial Y}{\partial X_{\rm s}})}{X_{\rm s}(Y - X_{\rm s}\frac{\partial Y}{\partial X_{\rm s}})}}. \tag{8}$$

We can also obtain y using Eq. (4) in the same way as in the Bistatic-IBST. We call Eqs. (8) and (4) the CMP-IBST. This transform corresponds to antenna scanning with a fixed midpoint between a pair of transmitting and receiving antennas, which keeps $X_{\rm a}$ at a constant value.

V. Difference between Bistatic-IBST and CMP-IBST

The Bistatic-IBST and proposed CMP-IBST are derived for a fixed gap and midpoint of antennas, respectively. These conditions correspond to different antenna scanning schemes, which is shown in Fig. ant. With regard to the Bistatic-IBST, the transmitting and receiving antennas are installed on a single platform. Both the antennas are scanned simultaneously in the same way. Note that this corresponds to a mono-static radar when the distance between the antennas is zero. As for CMP-IBST, the midpoint of the antennas is fixed while both the antennas are scanned in the opposite directions.

These antenna scanning schemes correspond to the use of different sections of the multi-static radar data as in Fig. bibst. In this figure, the horizontal and vertical axes are the transmitting and receiving antenna positions. Partial derivatives are

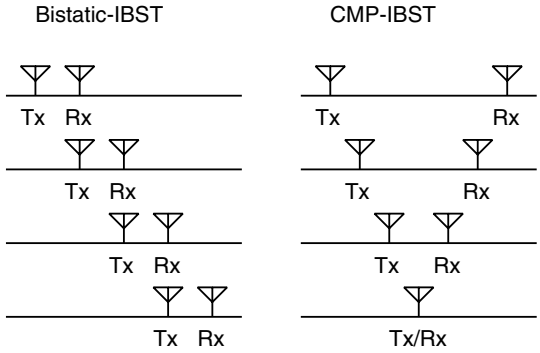

Fig. 2. Antenna scanning assumed for Bistatic-IBST and CMP-IBST.

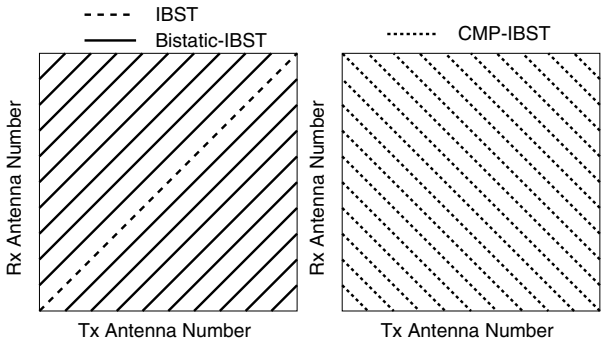

Fig. 3. Multistatic data sets used for the IBST, Bistatic-IBST and CMP-IBST.

calculated along these lines to obtain the images using the Bistatic-IBST or CMP-IBST. We see that the IBST is a special case of the Bistatic-IBST. We also see that CMP-IBST uses information that has never been used in the existing imaging methods.

VI. Performance Comparison of Bistatic-IBST and CMP-IBST

We show images generated by the Bistatic-IBST and CMP-IBST to compare their accuracies. As in Fig. 1, a circular target with a radius of 0.1 m is located at (1.5 m, 1.5 m) in the coordinate system with the origin at the center of the antenna array. We assume a 20-element array with intervals of 0.2 m. Though in actual measurement the waveforms are distorted owing to the antenna pattern, propagation and scattering process, we only consider additive white Gaussian noise for simplicity.

Figures 4, 5 and 6 show images generated with IBST, Bistatic-IBST and CMP-IBST in a noiseless environment. The solid lines in the figures show the actual target shape. The IBST uses only 20 signals out of $20 \times 20 = 400$ data sets by assuming mono-static measurement. Because of this, the image of IBST has a small number of estimation points. We see that the images of Bistatic-IBST and CMP-IBST are almost the same in a noiseless environment. Note that only the bottom part of the target is imaged in all cases because the antenna array is located below the target as in Fig. 1.

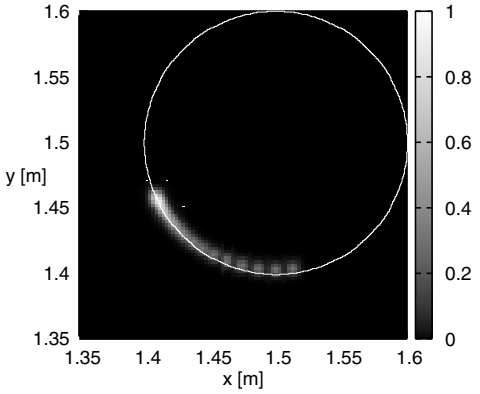

Fig. 4. Image obtained using the IBST for noiseless data.

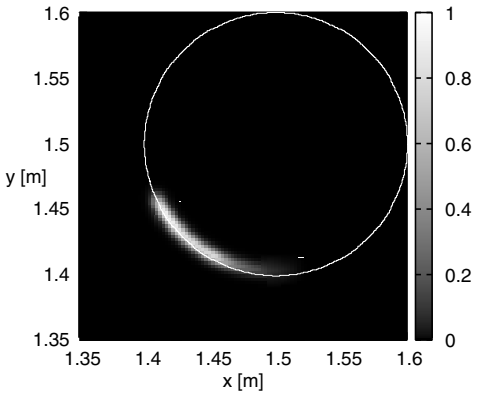

Fig. 5. Image obtained using the Bistatic-IBST for noiseless data.

Figs. 7, 8 and 9 show the images generated with IBST, Bistatic-IBST and CMP-IBST for a ranging root mean square (RMS) error of 1 mm. The image of IBST significantly deteriorates in this case because the number of estimation points is limited. On the other hand, the target shape is almost accurately estimated in the images of Bistatic-IBST and CMP-IBST. The image of the CMP-IBST is more sensitive to small noise than that of the Bistatic-IBST.

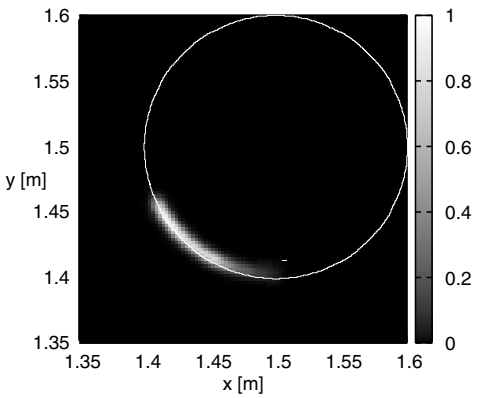

Fig. 6. Image obtained using the CMP-IBST for noiseless data.

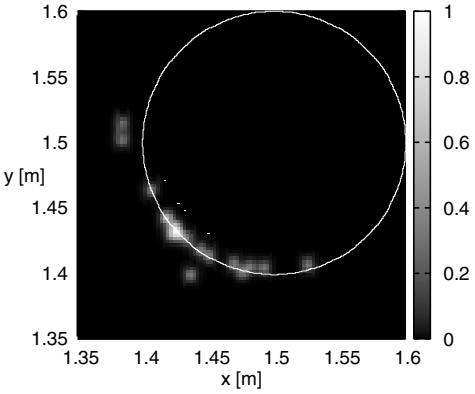

Fig. 7. Image obtained using the IBST for a ranging error of 1.0 mm.

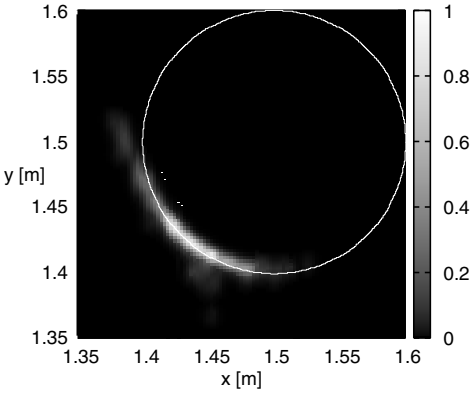

Fig. 8. Image obtained using the Bistatic-IBST for a ranging error of 1.0 mm.

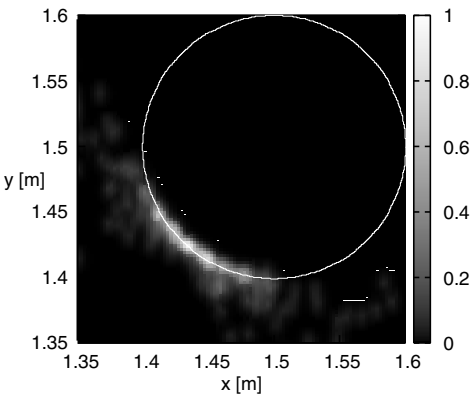

Fig. 9. Image obtained using the CMP-IBST for a ranging error of 1.0 mm.

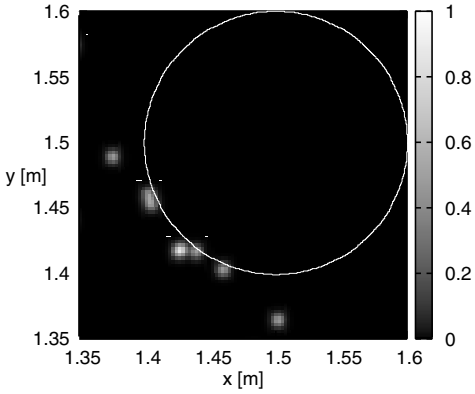

Fig. 10. Image obtained using IBST for a ranging error of 10.0 mm.

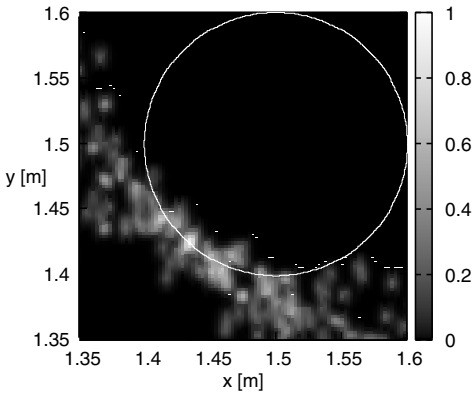

Fig. 11. Image obtained using Bistatic-IBST for a ranging error of 10.0 mm.

Figs. 10, 11 and 12 show the images of IBST, Bistatic-IBST and CMP-IBST for ranging RMS error of 10 mm. In this case, all the images are vague and we do not see a clear shape in any of them.

Figure 13 shows the imaging RMS error of Bistatic-IBST and CMP-IBST for the same antenna array and target used above. The imaging error is defined as the distance between the estimated point and the nearest point on the actual target. The noise is numerically generated with 10,000 patterns of seeds to statistically evaluate the error values. We see the CMP-IBST gives larger error than the Bistatic-IBST for a small ranging error. For a ranging RMS error larger than 40 mm, the imaging error of the CMP-IBST becomes smaller than that of the Bistatic-IBST. It can be said that the proposed CMP-

Fig. 12. Image obtained using CMP-IBST for a ranging error of 10.0 mm.

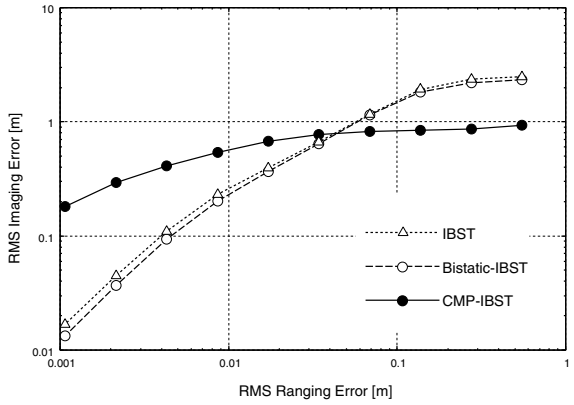

Fig. 13. Imaging accuracy for the Bistatic-IBST and CMP-IBST.

IBST enables more accurate imaging in severe conditions with low S/N.

We also see that the imaging error of the IBST is almost the same as that of the Bistatic-IBST in Fig. error2. Although some images of the IBST shown above look more degraded than those of the Bistatic-IBST, the actual difference is only about the number of estimated points.

VII. Conclusions

We investigated the imaging methods for UWB multi-static radars. In addition to the existing IBST and Bistatic-IBST, we derived a new closed-form solution, the CMP-IBST, and compared their performance with computer simulations. The simulations demonstrated that the conventional methods and the proposed method give almost the same accuracy. It was also shown that the conventional Bistatic-IBST outperforms in high S/N conditions, and the CMP-IBST outperforms in low S/N conditions.

References

[1] A. G. Yarovoy, T. G. Savelyev, P. J. Aubry, P. E. Lys, L. P. Ligthart, "UWB array-based sensor for near-field imaging," IEEE Transactions on Microwave Theory and Techniques, vol. 55, no. 6, part 2, pp. 1288-1295, June 2007.

[2] Y. Wang, Y. Yang, A. E. Fathy, "Experimental assessment of the cross coupling and polarization effects on ultra-wide band see-through-wall imaging reconstruction," IEEE MTT-S International Microwave Symposium Digest, pp. 9–12, June 2009.

[3] A. Nelander, "Switched array concepts for 3-D radar imaging," Proc. 2010 IEEE Radar Conference, pp. 1019–1024, 2010.

[4] T. Sakamoto and T. Sato, "A target shape estimation algorithm for pulse radar systems based on boundary scattering transform," IEICE Transaction on Communications vol. E87-B, no. 5, pp. 1357–1365, May 2004.

[5] T. Sakamoto and T. Sato, "A fast algorithm of 3-dimensional imaging for pulse radar systems," Proc. 2004 IEEE AP-S International Symposium and USNC/URSI National Radio Science Meeting, vol. 2, pp. 2099–2102, June, 2004.

[6] S. Kidera, Y. Kani, T. Sakamoto and T. Sato, "A fast and high-resolution 3-D imaging algorithm with linear array antennas for UWB pulse radars," IEICE Trans. on Commun., vol. E91–B, no. 8, pp. 2683–2691, Aug. 2008.

[7] T. Sakamoto and T. Sato, "Code-division multiple transmission for high-speed UWB radar imaging with an antenna array," IEEE Trans. on Geoscience and Remote Sensing, vol. 47, no. 4, pp. 1186–1179, Apr. 2009.